



Published in final edited form as:

Cancer Res. 2015 April 1; 75(7): 1287–1297. doi:10.1158/0008-5472.CAN-14-2444.

## **PARD3 Inactivation in Lung Squamous Cell Carcinomas Impairs STAT3 and Promotes Malignant Invasion**

**Ester Bonastre<sup>1</sup>, Sara Verdura<sup>1</sup>, Ilse Zondervan<sup>2</sup>, Federica Facchinetti<sup>3</sup>, Sylvie Lantuejoul<sup>4</sup>, Maria Dolores Chiara<sup>5</sup>, Juan Pablo Rodrigo<sup>5</sup>, Julian Carretero<sup>6</sup>, Enric Condom<sup>7</sup>, Agustin Vidal<sup>7</sup>, David Sidransky<sup>8</sup>, Alberto Villanueva<sup>9</sup>, Luca Roz<sup>3</sup>, Elisabeth Brambilla<sup>4</sup>, Suvi Savola<sup>2</sup>, and Montse Sanchez-Cespedes<sup>1</sup>**

<sup>1</sup>Genes and Cancer Group, Cancer Epigenetics and Biology Program (PEBC), Bellvitge Biomedical Research Institute (IDIBELL), Hospitalet de Llobregat, Barcelona, Spain <sup>2</sup>MRC-Holland, Willem Schoutenstraat, the Netherlands <sup>3</sup>Tumor Genomics Unit, Department of Experimental Oncology and Molecular Medicine, Fondazione IRCCS Istituto Nazionale Tumori, Milan, Italy <sup>4</sup>Department of Pathology, Institut Albert Bonniot, INSERM U823, University Joseph Fourier, CHU, Grenoble Hôpital Michallon, Grenoble, France <sup>5</sup>Department of Otolaryngology of the Hospital Universitario Central de Asturias, Oviedo, Spain <sup>6</sup>Department of Physiology, Faculty of Medicine and Odontology, University of Valencia, Spain <sup>7</sup>Pathology Department, Bellvitge Hospital, Hospitalet de Llobregat, Barcelona, Spain <sup>8</sup>Departments of Otolaryngology-Head and Neck Surgery, Johns Hopkins University School of Medicine, Baltimore, Maryland <sup>9</sup>Translational Research Laboratory, Catalan Institute of Oncology (ICO)-IDIBELL, Barcelona, Spain

### **Abstract**

Correct apicobasal polarization and intercellular adhesions are essential for the appropriate development of normal epithelia. Here, we investigated the contribution of the cell polarity regulator *PARD3* to the development of lung squamous cell carcinomas (LSCC). Tumor-specific *PARD3* alterations were found in 8% of LSCCs examined, placing *PARD3* among the most common tumor suppressor genes in this malignancy. Most PAR3-mutant proteins exhibited a

---

Corresponding Author: Montse Sanchez-Cespedes, Bellvitge Biomedical Research Institute (IDIBELL), Hospitalet de Llobregat, Barcelona 08908, Spain. Phone: 34-93-260-71-32; Fax: 34-93-260-72-19; mscspedes@idibell.cat.

**Note:** Supplementary data for this article are available at Cancer Research Online (<http://cancerres.aacrjournals.org/>).

#### **Disclosure of Potential Conflicts of Interest**

No potential conflicts of interest were disclosed.

Array data have been deposited in the Gene Expression Omnibus under accession reference GSE51506.

#### **Authors' Contributions**

**Conception and design:** E. Bonastre, M. Sanchez-Cespedes

**Development of methodology:** E. Bonastre, S. Verdura, F. Facchinetti, A. Villanueva, E. Brambilla, S. Savola

**Acquisition of data (provided animals, acquired and managed patients, provided facilities, etc):** E. Bonastre, S. Verdura, I. Zondervan, S. Lantuejoul, M.D. Chiara, J.P. Rodrigo, E. Condom, A. Vidal, D. Sidransky, A. Villanueva, L. Roz, E. Brambilla, M. Sanchez-Cespedes

**Analysis and interpretation of data (e.g., statistical analysis, biostatistics, computational analysis):** E. Bonastre, S. Verdura, I. Zondervan, M.D. Chiara, J.P. Rodrigo, J. Carretero, E. Condom, A. Vidal, A. Villanueva, L. Roz, M. Sanchez-Cespedes

**Writing, review, and/or revision of the manuscript:** E. Bonastre, A. Vidal, L. Roz, E. Brambilla, M. Sanchez-Cespedes

**Administrative, technical, or material support (i.e., reporting or organizing data, constructing databases):** S. Verdura, I. Zondervan

**Study supervision:** M. Sanchez-Cespedes

relative reduction in the ability to mediate formation of tight junctions and actin-based protrusions, bind atypical protein kinase C, activate RAC1, and activate STAT3 at cell confluence. Thus, *PARD3* alterations prevented the formation of contacts between neighboring cells and the subsequent downstream signaling. Notably, reconstituting PAR3 activity *in vivo* reduced tumor-invasive and metastatic properties. Our findings define *PARD3* as a recurrently inactivated cell polarity regulator in LSCC that affects tumor aggressiveness and metastasis.

## Introduction

Lung cancer is among the most frequent and deadly types of cancer in western countries. Lung tumors carry alterations at known genes, some of them highly specific to the tumor histopathology (1, 2). Lung adenocarcinomas (LAC) are the best characterized, whereas the gene alteration profile of lung squamous cell carcinomas (LSCC) is less well understood (1–3). Inactivation of *TP53* and *CDKN2A* and amplification of *MYC* are among the most common alterations found in LSCCs, whereas alterations at other genes are only occasionally observed (2–4). The paucity of information about LSCC genetics has promoted efforts to find novel genes that are altered in this type of lung cancer. This has enabled the identification of focal amplification at *FGFR1*, *SOX2*, *TFDP1*, and *CTNND1* and activating mutations at *DDR2* (5–8). More recently, genome-wide sequencing has revealed mutations at other genes in LSCCs, including loss-of-function mutations in the *HLA-A*, *NFE2L2*, and *KEAP1* (9). However, most of these alterations affect a small percentage of lung LSCCs.

Homozygous deletion is a common mechanism for inactivating tumor suppressor genes (10, 11). Using genome-wide strategies, Rothenberg and colleagues (12) found intragenic deletions at *PARD3* in cancer cell lines and primary tumors from head and neck squamous cell carcinomas (HNSCC), esophageal carcinomas, and glioblastomas. The *PARD3* (from “partitioning defective”) gene encodes PAR3, first identified in *C. elegans* (13), and now found in almost every organism, including mammals (14). In *D. melanogaster*, Par3 functions as a scaffolding protein involved in cell polarity and is the earliest known landmark for establishing epithelial polarity in the embryo (15). The best known role of PAR3 in mammals is the formation in the epithelia of the tight junctions, a specialized type of intercellular adhesion complex that defines the apical–lateral border of the cell membrane compartments (14–16). The PAR3 protein acts in a complex, the PAR polarity complex, comprising PAR3, PAR6, atypical protein kinase C (aPKC), and cell division control protein 42 (CDC42; ref. 14).

As further evidence of the role of PAR3 in cancer development, it has recently been shown that mice with *Pard3* conditionally deleted in the skin epidermis have a strong predisposition to form keratoacanthomas, a common cutaneous tumor in humans that is thought to arise from a different cellular origin than squamous cell carcinomas (17). Furthermore, depletion of Par3 in mammary gland cells is evidence of increased cell growth and the formation of metastasis (18). Here, we aimed to determine whether *PARD3* has a role in LSCC development.

## Materials and Methods

### Cell lines and tumor samples

Fifty-one lung cancer cell lines were studied (Supplementary Table S1). The cell lines were authenticated by testing for *TP53* and other mutations (e.g., *SMARCA4*, *STK11*, etc.). The mutations were genotyped before starting the experiments and were in agreement with those provided in public databases. Tumors were obtained from the Johns Hopkins University School of Medicine (Baltimore, MD), the CNIO Tumour Bank Network (Madrid, Spain), the Fondazione IRCCS Istituto Nazionale Tumori (Milan, Italy), and the Hospital Universitario Central de Asturias (Oviedo, Spain).

### Direct sequencing and MS-MLPA of *PARD3*

For mutation screening of the *PARD3*, exons 1 to 26 (*H. sapiens* chromosome 10 reference assembly NC\_019619) were amplified. The sequence of primers used is provided in Supplementary Table S2.

Methylation-specific multiplex ligation-dependent probe amplification (MS-MLPA) was used to determine the presence of intragenic homozygous deletion and promoter hypermethylation of the *PARD3* gene. The MLPA analysis was carried out using SALSA P448-A1-lot0811 *PARD3* probe mix and MLPA reagents (MRC-Holland) following the MS-MLPA protocol (see Supplementary Methods).

### Microarray analysis

RNA (100 ng) was used for the gene expression microarray employing RNA Integrity. Values ranged from 9.0 to 10.0 (Lab-chip technology with an Agilent 2100 Bioanalyzer). For labeling, we used the commercial One-Color Microarray-Based Gene Expression Analysis (version 5.5) Kit, following the manufacturer's instructions (Agilent manual G4140-90050, February 2007). Hybridization was performed on the Human Gene Expression v2 microarray 8 × 60 K (Agilent microarray design ID 014850, P/N G4112F).

## Results

### *PARD3* is somatically and biallelically inactivated in LSCCs

We searched in databases for homozygous deletions and concomitant decreases in gene expression in cancer cell lines and observed that several members of the PAR family of proteins are deleted in different types of cancer (Wellcome Trust Sanger Institute's Cancer Cell Line Project website; ref. 12). Here, we have focused on one of these genes: *PARD3*. After confirming the homozygous deletions at *PARD3* in the NCI-H157 (hereafter H157) cell line (Supplementary Fig. S1A and S1B), we sequenced its coding region in 51 lung cancer cell lines. We found another cell line, PC10, with two *PARD3* alterations: a c.2581A>T change, which causes an amino acid substitution, and the intronic variant c.223-4C>G, whose effect is unknown. Despite being in heterozygosis, the missense change was predominant at the mRNA level (Fig. 1A). This suggests that the c.223-4C>G variant affects splicing and triggers nonsense-mediated decay of this mRNA, thus implying that the PC10 cells carry biallelic inactivation of *PARD3*.

The H157 and PC10 are of the LSCC type. This is consistent with a previous observation about the presence of *PARD3* mutations in primary HNSCCs (12), which are etiologically and molecularly very similar to LSCCs (19). Given this background, we decided to screen for *PARD3* alterations in LSCCs. In addition to Sanger sequencing, we used the MLPA assay to search for intragenic homozygous deletions. The deletion at H157 was clearly observed by MLPA (Supplementary Fig. S1C).

Overall, we found tumor-specific *PARD3* alterations in 8% of the LSCCs. Interestingly, some of the alterations resulted in in-frame rearrangements that predict shorter proteins (Table 1). Noticeably, all the alterations at *PARD3* rendering in-frame deletions only affected common exons. In addition to mutations predicting shorter forms or the complete absence of PAR3 protein expression, we identified missense alterations at *PARD3*. Some of these amino acid substitutions are predicted to be deleterious by the polymorphism phenotyping tool (20). We also tested for LOH and confirmed the “two hit” hypothesis for tumor suppressors (Fig. 1; and Supplementary Fig. S2; ref. 21). The location of the different mutations within the domains of the PAR3 protein is detailed in Fig. 1D. All known SNPs and germ-line variants found are listed in Supplementary Table S3. Information on the mutation status of *PARD3* and the different tumor and patient characteristics is provided in Supplementary Table S4.

Because CpG promoter hypermethylation is a mechanism for gene inactivation, we designed MLPA probes to assess this alteration at the promoter of *PARD3*. One of the probes indicated the presence of CpG methylation, which was confirmed by bisulfite sequencing, in a subset of lung cancer cell lines (Supplementary Fig. S3). However, the presence of methylation at these sites was not correlated with the loss of protein expression, so we discounted the possibility that this mechanism accounts for *PARD3* loss of expression in lung cancer.

### Effect of PAR3-mutant proteins on cell growth suppression

The *PARD3* structure is complex because it has alternative splice sites and two different stops, resulting in multiple PAR3 protein isoforms, some of which are detectable by Western blot (Supplementary Fig. S1B). We determined that the transcript NM\_001184785.1 was the most abundant in normal lung (Supplementary Fig. S4).

To assess the effect of the *PARD3* mutations in LSCC, we cloned the most abundant wild-type and five mutant transcripts and expressed them in H157 cells (Fig. 2A). Of notice, the antiPAR3 antibody did not recognize the p.D41\_E689del mutant protein (Supplementary Fig. S5A). First of all, we evaluated the ability of the wtPAR3 and the PAR3-mutant proteins to suppress cell growth in the H157 cell line. Compared with the wtPAR3, the PAR3 mutants, especially p.D41\_R74del and p.D41\_E689del, were significantly less able to suppress cell growth (Fig. 2B).

## Effect of PAR3-mutant proteins on intercellular contacting and downstream target activation

We determined the intracellular location of the ectopically expressed PAR3 proteins. We observed that, although the wtPAR3 and the amino acid change mutants were located in the cell membrane, at cell–cell contacts, and in the cytoplasm, the p.D41\_R74del and p.D41\_E689del PAR3 proteins were predominantly located in the cytoplasm (Fig. 2C).

In addition to PAR3, the PAR complex comprises PAR6, aPKC, and CDC42. aPKC binds PAR6 that tethers the kinase to the tight junction where it interacts with PAR3. Once there, PAR3 is phosphorylated by aPKC, which stabilizes PAR3 at the tight junctions (22). We tested whether the PAR3 mutations affect its interaction with aPKC. Similar levels of endogenous aPKC were recovered from all the hemagglutinin immunoprecipitates, except in the case of the p.D41\_E689del mutant, for which no aPKC was detected (Fig. 2D). Therefore, the large deletion was the only mutation that impaired the binding of PAR3 with aPKC.

To evaluate the effects of the *PAR3* inactivation in detail, we constructed H157-derived isogenic cell lines that express stable and doxycycline-inducible wtPAR3 (H157tr-wtPAR3 hereafter) and the mutants p.D41\_R74del, p.R345H, p.T861S, and p.I1043M (hereafter, H157tr-D41\_R74del, H157tr-R345H, H157tr-T861S, and H157tr-I1043M, respectively; Fig. 3A). Immunofluorescence confirmed the ectopic expression of PAR3 in about 40% to 80% of the cell population (Supplementary Fig. S5B). The induction of PAR3 expression in the H157tr-wtPAR3 cells resulted in a decreased number of colonies, supporting the observations above (Fig. 2B), and discarded a bias due to differences in transfection efficiency (Supplementary Fig. S5C). Further, we tested the involvement of PAR3 in cell proliferation and migration, using the MTT and the xCELLigence system assays, respectively. Our results show a significant reduction of cell migration capability but not of cell proliferation, in the H157tr-wtPAR3 as compared with the control cells (Fig. 3B and Supplementary Fig. S5D). These observations support a role of *PAR3* inactivation in tumor invasiveness.

Given the involvement of PAR3 in the formation of tight junctions (14), we explored the capability of the various PAR3-mutant proteins to colocalize with the tight junction protein, Zona occludens protein 1 (ZO-1). The analysis confirmed that wtPAR3 colocalized with ZO-1 and restored the capability of ZO-1 to accumulate at high density in the cell membrane at cell–cell contact regions. Similarly, the PAR3 proteins carrying amino acid substitutions exhibited strong coimmunolocalization of PAR3 and ZO-1 at the cell–cell contacts and an accumulation of ZO-1 in the cell membrane, as opposed to the H157tr and H157tr-D41\_R74del cells (Fig. 3C).

For the appropriate control of cell and cytoskeletal polarity, the PAR complex is connected to various signaling pathways, including that of RhoGTPases (22, 23). It is known that PAR3 interacts with the RacGEF, TIAM1, and that this interaction is important for regulating actin protrusions, e.g., lamellipodia and filopodia, in various types of migratory mammalian cells (23–25). Consistent with this, we observed that, when sparsely seeded, cells expressing ectopic wtPAR3 formed actin-rich protrusions oriented toward other cells,

with which cell–cell contacts were established (Fig. 3D). All protrusions were formed of filamentous actin and colocalized with the F-actin marker, phalloidin (Supplementary Fig. S5E). There were significantly fewer protrusions in those cells lacking PAR3 or in the H157tr-D41\_R74del and H157tr-R345H cells. To rule out cell-specific bias, we determined whether the behavior was reproduced in the glioma-derived and *PARD3*-deficient T98G cells (12). We generated T98G-derived isogenic cell lines that expressed stable and doxycycline-inducible wt and mutants of *PARD3* (Supplementary Fig. S6A and S6B). In agreement with observations made in the H157-derived cells, the T98Gtr-wtPAR3 and the amino acid substitution mutants showed strong immunostaining at the cell–cell contacts, whereas the T98Gtr-D41\_R74del accumulated at the cytoplasm (Supplementary Fig. S6C). The ability to form protrusions also differed between wt- and mutant PAR3–expressing cells (Supplementary Fig. S6D).

The interaction of the PAR3 complex with TIAM1 also leads to the activation of the small GTPase, RAC1, whereas the inhibition of the formation of the complex results in RAC1 inactivation (22, 24). In contrast with this, others reported a constitutively active Rac1 in cells lacking Par3 (25). Here, we found that restitution of PAR3 in the H157tr-wtPAR3 cells increases the levels of the GTP-RAC1 fraction. This also occurred in the H157tr-R345H and H157tr-T861S mutant cells, but not in the H157-derived cells expressing other PAR3-mutant proteins (Fig. 3E). Therefore, our results indicate that PAR3 is required to promote the activation of RAC1. Intriguingly, the activation of RAC1 following restitution of wtPAR3 was not observed in the T98G-derived cells.

We noted that the levels of the p.D41\_R74del protein, but not the mRNA, were low as compared with the wild type (Fig. 3A and Supplementary Fig. S6B). To determine whether these observations were a consequence of active degradation, we treated the cells with MG132, which is a very efficient proteasome inhibitor (26), and with N-[N-(N-Acetyl-L-leucyl)-L-leucyl]-L-norleucine (ALLN), which inhibits neutral cysteine proteases and the proteasome. The levels of the p.D41\_R74del protein were substantially higher after the addition of either MG132 or ALLN, whereas the levels of the wtPAR3 protein remained high in the H157- and T98G-derived cells (Fig. 3F and Supplementary Fig. S6E). Interestingly, the accumulation of p.D41\_R74del protein was more evident after treatment with the MG132 than with the ALLN inhibitor. Altogether, the results demonstrate that the p.D41\_R74del suffers from protein degradation by the proteasome. Despite this, the levels of p.D41\_R74del protein after 24 hours of doxycycline induction were in the range of the endogenous levels of PAR3 (Supplementary Fig. S7A). Because of that, it is unlikely that the relatively lower abundance of this mutant protein would affect its subcellular localization or other parameters and, thus, we considered that the H157tr-D41\_R74del cells are suitable for carrying out a molecular study of the effects of the CR1 region on PAR3 functionality.

### **The gene expression signature of PAR3 is enriched in transcripts involved in cell adhesion and the cell junction**

Next, we compared the gene expression profiles of the H157tr control and the H157tr-D41\_R74del with that of the H157tr-wtPAR3 cells after induction of PAR3 expression.



About 150 genes were differentially expressed (Supplementary Table S5) in the H157tr-wtPAR3 cells. Gene ontology analysis linked the PAR3 gene expression signature to functions associated with cell adhesion, cell motion, and the cell junction (Fig. 4A and B). We selected six transcripts representing different gene functions to test how the different mutants of PAR3 affect the expression levels of these genes. Interestingly, the H157tr-I1043M cells showed the same gene expression profile for five of the six transcripts as the H157tr or the H157tr-D41\_R74del cells, which highlights its inactivating nature (Fig. 4C). In contrast, the expression levels of the selected genes in the H157tr-p.R345H and H157tr-p.T861S mutants had a variable pattern, halfway between that of the mock and wild-type cells.

### PAR3 is required to activate STAT3 upon cell–cell contact

Among the transcripts that were upregulated in the H157tr-wtPAR3 cells were also cytokines and targets of STAT3 (Fig. 4B), suggesting a PAR3–STAT3 functional relationship. We therefore decided to explore this further.

First, we compared the gene-expression profile of the H157tr-wtPAR3 cells with that of two human cancer cell lines after knockdown of STAT3 (27) and observed an inverse association (Fig. 4D). Phosphorylation of STAT3 at the tyrosine 705 (pY-STAT3) induces its activation and thus dimerization, nuclear translocation, and DNA binding (28). We observed that the levels of pY-STAT3 were higher in the H157tr-wtPAR3 cells than in the control cells and in the mutant counterparts (Fig. 4E). The phosphorylation levels of other PAR3-related proteins, such as aPKC, remain unchanged. The increase in pY-STAT3 following restitution of PAR3 was particularly evident when cells were grown at high density (Fig. 4F), which is consistent with previous reports showing that STAT3 activity dramatically increases with cell confluence (29, 30). These observations were confirmed using calcium depletion experiments. Withdrawal of calcium from the medium causes rapid loss of cell–cell junctions (25), a process that can be reversed by readdition of calcium (a calcium switch). A strong decrease in pY-STAT3 was observed after calcium depletion in the H157tr-wtPAR3 cells (Fig. 4F). The levels of pY-STAT3 were recovered 24 hours after calcium readdition (Supplementary Fig. S7B). Furthermore, we depleted *PAR3* expression in lung cancer cells with wild-type endogenous PAR3, such as the H1299 and H2170 cells, and observed a decrease in the levels of pY-STAT3 in high-density cell cultures (Fig. 4G). Taken together, these observations suggest that, upon cell–cell contact, the formation of tight junction triggers an increase in the activation of STAT3, in a process that requires the activity of wtPAR3. Similarly to what it was observed for RAC1, the activation of STAT3 following restitution of PAR3 was not evident in the T98G cells, which could reflect differences in the cell and tissue of origin. The LSCC cells derive from the respiratory epithelia, a tissue that relies strongly on tight junctions for maintaining epithelial integrity (31). In this case, the loss of tight junctions may permit contact-inhibited cells to separate from neighboring cells and proliferate and invade other tissues. However, the T98G derive from glia cells of the nervous tissue, where the regulation of cell–cell contact is different as it is in the respiratory epithelia.

### Restoration of wtPAR3 reduces tumor invasiveness and prevents formation of metastasis *in vivo*

To investigate the tumorigenicity of the H157tr-wtPAR3 and H157tr cells *in vivo*, we examined their capacity to grow orthotopically and to form tumors in the lung parenchyma of athymic nude mice. Animals were randomly assigned to two groups, each containing 11 mice, and were implanted with the H157tr-wtPAR3 and H157tr cells. We counted the number of cancer lesions in the lung and in the liver, an organ that is a common target for metastasis in lung cancer patients. Both groups of mice developed orthotopic tumors and the H157tr-wtPAR3 tumors efficiently expressed wtPAR3 and higher levels of pY-STAT3 (Fig. 5A). Liver metastases and cancer lesions in the lung were detected in both groups of mice. The generation of liver metastasis indicates that this model closely follows the natural pathology of metastasis development from lung primary tumor growth. Overall, we observed that the wtPAR3-expressing tumors had significantly fewer lesions in the lungs and metastases to the liver than mice whose tumors did not express PAR3 (Fig. 5B).

These observations prompted us to generate another mouse model to test, specifically, the differences in the metastatic capability of the cells. Mice were divided into two groups: those carrying H157tr-wtPAR3 ( $n = 7$ ) or H157tr ( $n = 6$ ) cells, implanted into the spleen of the animals. We then measured the number and size of the metastases generated in the lungs and livers. We also confirmed the effective induction of ectopic wtPAR3 and increased pY-STAT3 levels (Fig. 5C). Significantly fewer metastatic lesions were found in the lungs of mice carrying H157tr-wtPAR3 (Fig. 5D). In addition, we observed that cancer lesions that arose in the liver of the mice implanted with the H157tr-wtPAR3 were smaller and round in shape, suggesting a reduced invasive capability, than the liver lesions found in the H157tr group of mice (Fig. 5E).

### Patterns of PAR3 immunostaining in lung primary tumors and in HNSCCs

Next, we performed immunohistochemistry of PAR3 in lung tumors and HNSCCs. We included HNSCCs because these tumors are histologically similar to that of LSCC (19). A collection of about 190 lung primary tumors of different histopathologies, i.e., LACs and LSCCs and a panel of 262 HNSCCs, were tested. As expected, those lung tumors carrying *PAR3* mutations predicting no protein expression were negative for PAR3 immunostaining. On the other hand, the tumors carrying the p.D41\_R74del and p.D41\_E689del showed moderate and negative immunostaining of PAR3, respectively (Supplementary Fig. S8A). This is consistent with the observations made in Western blots and in immunofluorescences.

Very strong levels of PAR3 were detected in some of the tumors that were wild type for *PAR3*. PAR3 immunostaining was evident in the cell membrane and the cytoplasm of these tumors (Fig. 6A and B). We observed that more LACs exhibited strong immunostaining than did LSCCs and HNSCCs (Fig. 6C). Intriguingly, in some lung tumors, predominantly LACs, the strong PAR3 immunostaining appeared as punctuate clusters (Fig. 6A). Although we do not know the biologic significance, it is interesting to note that similar punctuate clusters containing PAR3 have previously been observed in Caco-2 cells derived from colorectal adenocarcinomas (32, 33). Likewise, in some of the HNSCCs, there was a



notable heterogeneous pattern of PAR3 immunostaining, whereby staining was stronger in those regions where the tumor became invasive (Supplementary Fig. S8B).

In the HNSCCs, we examined the pattern of the PAR3 immunostaining in normal epithelia and in preneoplastic lesions, adjacent to tumor regions. In the normal epithelia, the PAR3 protein was detected predominantly in the apical region of the cells from the basal layer. The hyperplastic and dysplastic lesions exhibited a similar pattern. The distribution of the PAR3 immunostaining was similar among the two different types of preneoplastic lesions, although the number of samples is too small to draw definitive conclusions (Supplementary Fig. S8B).

Lung tumors of patients with high and moderate levels of PAR3 were larger than those showing negative or low levels of PAR3. No associations were observed between the different levels of PAR3 and the development of distant or lymph node metastasis (Supplementary Fig. S8C). Finally, we performed immunohistochemistry of pY-STAT3 in a panel of 88 lung cancers specimens, which included most tumors tested for PAR3 immunostaining and for *PARD3* mutations. As expected, *PARD3*-mutant tumors were negative for pY-STAT3 immunostaining. Similarly to PAR3, we observed that more LACs exhibited strong immunostaining of pY-STAT3 than did LSCCs (Fig. 6D and Supplementary Table S4).

## Discussion

We discovered recurrent tumor-specific inactivating alterations of the polarity-related gene *PARD3* in 8% of LSCCs. This frequency is very similar to that of other well-established tumor suppressor genes, such as *PTEN* (2). Homozygous deletions in other components of the PAR3 complex have been found in various types of cancer cells (12), indicating that abnormalities in the control of cell polarity are relatively widespread in cancer. It is worth mentioning that the tumor suppressor gene *LKB1*, which is commonly inactivated in lung cancer (34), also controls cell polarity and has been associated with the PAR complex (16, 35). However, *LKB1* is deleted in the H157 cells (2), which argues against the hypothesis that inactivation of *LKB1* or *PARD3* is functionally equivalent in cancer development.

The p.D41\_R74del and the p.D41\_E689del proteins had an impaired ability to localize at the edge of the cell membrane, preventing colocalization with ZO-1. The 33 amino acids missing from the p.D41\_R74del mutants are located within the control region 1 (CR1) domain, attesting to the involvement of this region in correctly positioning PAR3 at the edge of the cell membrane. This is consistent with previous observations in the *PARD3* homolog in *Drosophila* (33, 36). The aberrant location of the p.D41\_R74del in the cytosol could explain its degradation by the proteasome, as our current results show. The p.R345H, p.D41\_R74del mutations showed a significantly reduced ability to form large filamentous actin protrusions. These filaments, probably lamellipodia and filopodia, are involved in substrate adhesion and in directed locomotion toward establishing contacts between epithelial cells. The p.R345H, p.D41\_R74del mutations affect the PDZ1 domain of PAR3, which is required to form a complex with the discoidin domain receptor 1 (DDR1) and with PAR6 to antagonize ROCK-driven actomyosin contractility (37–40). DDR1 has also been

found to prevent the activation of STAT3 (41). Thus, the fewer large actin protrusions observed in these mutants could be a consequence of defective binding to DDR1. It is worth remembering that oncogenic mutations at DDR1 and DDR2 have been found in breast cancer and LSCCs, respectively (7, 40).

The T861S substitution is located near the aPKC binding domain, close to residues that are phosphorylated by aPKC (S827/S829) or Rho-kinase (T833; refs. 37, 38). Phosphorylation at these residues reduces the affinity for aPKC/PAR6, thereby suppressing the activity of the PAR complex (18, 37–39). Although in our study only the p.D41\_E689del mutant PAR3 failed to bind aPKC, we cannot rule out the possibility that the T861S mutation affects the affinity of interaction with other partners. The I1043M mutation is located in the coiled-coil domain, whose function is unknown.

Restitution of PAR3 led to a pattern of gene expression that is compatible with its role in cell adhesion and polarity and included transcriptional targets of STAT3. This was correlated with an increase in the activation of STAT3, especially when cells were grown at high density. Our findings are consistent with those showing the involvement of PAR3 in the activation of RAC1 (37), which is required to promote STAT3 activation (42). However, the presence of activating mutations at STA73 in some leukemias attests to an oncogenic role for STAT3 (43). The reasons why a tumor suppressor, PAR3, would promote the activity of an oncogene, STAT3, are puzzling. Patterns of STAT3 activation differ, resulting from the formation of tight intercellular interactions following a transitory and regulated pattern (30), whereas most *STAT3* mutations render a constitutively active STAT3 (43). Moreover, STAT3 can act as a negative regulator of tumor growth, in the context of thyroid cancer, indicating that the activation of STAT3 is not always oncogenic (44). The formation of tight intercellular contacts may not be as important in nonepithelial tissues. Supporting this view, the glioma-derived cells T98G yielded no evidence of STAT3 activation upon PAR3 restitution. Figure 6E summarizes the functions that were altered in the PAR3-mutant proteins, and provides a schematic model of the pathways and downstream targets that would be activated during cell–cell recognition and during the formation of cell–cell contacts.

Consistent with the findings from a previous mouse model in which the depletion of Par3 promoted the formation of metastasis (18), here we show, in two different *in vivo* models, that the restitution of PAR3 reduced the capability to develop metastasis. This is compatible with the participation of PAR3 in promoting intercellular recognition and interactions. The immunostaining analysis in the LSCCs and in HNSCCs revealed no correlation between the levels of PAR3 and the presence of metastasis. This does not discount a role of PAR3 in promoting metastasis, because other components of the PAR3 complex can be altered in the tumors. In this regard, we believe that the strong and aberrant PAR3 immunostaining found in some of the lung tumors, wild type for *PARD3*, reflects the operation of feedback mechanisms derived from gene alterations at other key point controllers of the PAR3 complex or pathway.

In conclusion, we report recurrent and tumor-specific inactivation of *PARD3* in LSCC, which leaves little doubt that it acts as a *bona fide* tumor suppressor gene. Our findings also

highlight how *PARD3* inactivation contributes to LSCC development and metastasis through the abrogation of some important properties of epithelial cells, such as cell–cell recognition and the formation of cell contacts.

## Supplementary Material

Refer to Web version on PubMed Central for supplementary material.

## Acknowledgments

The authors acknowledge the technical assistance of Patricia Cabral (Genes and Cancer Group) at IDIBELL and of Dolores Moreno at the Human Pathology Department of the Hospital Universitario de Bellvitge.

### Grant Support

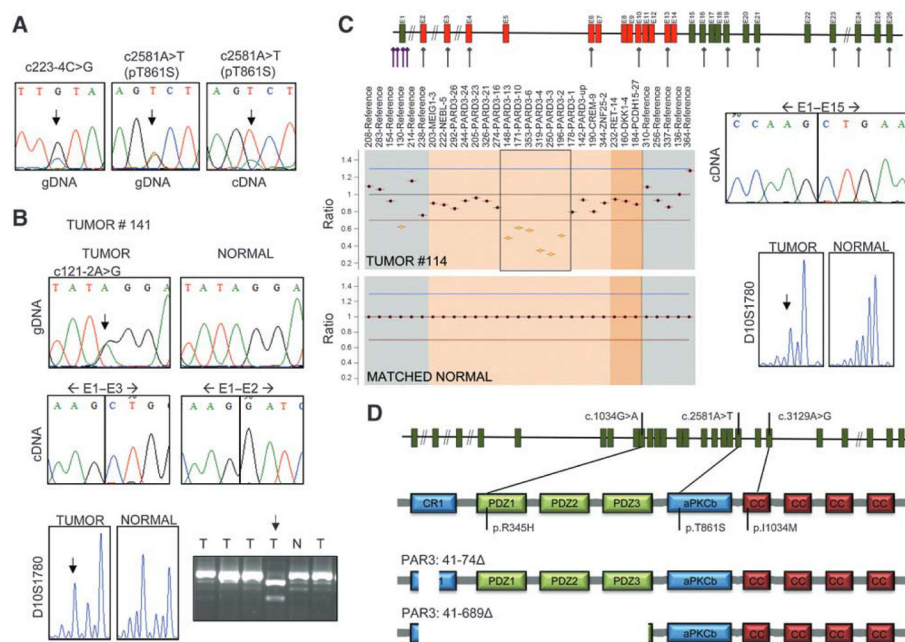
This work was supported by Spanish grants SAF2011-22897, RTICCs [RD12/0036/0045 (M. Sanchez-Cespedes) and RD12/0036/0015 (M.D. Chiara)], the Fondo de Investigacion Sanitaria (FIS PI11/929; M.D. Chiara and J.P. Rodrigo), the European Community's Seventh Framework Programme (FP7/2007–13), under grant agreement n°HEALTH-F2-2010-258677–CURELUNG, and grants from the Associazione Italiana per la Ricerca sul Cancro (AIRC IG9227 and IG13403; L. Roz). E. Bonastre is supported by a fellowship from the Spanish MINECO.

## References

1. Ding L, Getz G, Wheeler DA, Mardis ER, McLellan MD, Cibulskis K, et al. Somatic mutations affect key pathways in lung adenocarcinoma. *Nature*. 2008; 455:1069–75. [PubMed: 18948947]
2. Blanco R, Iwakawa R, Tang M, Kohno T, Angulo B, Pio R, et al. A gene-alteration profile of human lung cancer cell lines. *Hum Mutat*. 2009; 30:199–206. [PubMed: 19472407]
3. Sanchez-Cespedes M. Lung cancer biology a genetic and genomic perspective. *Clin Transl Oncol*. 2009; 11:263–9. [PubMed: 19451058]
4. Medina PP, Romero OA, Kohno T, Montuenga LM, Pio R, Yokota J, et al. Frequent BRG1/SMARCA4-inactivating mutations in human lung cancer cell lines. *Hum Mutat*. 2008; 29:617–22. [PubMed: 18386774]
5. Weiss J, Sos ML, Seidel D, Peifer M, Zander T, Heuckmann JM, et al. Frequent and focal FGFR1 amplification associates with therapeutically tractable FGFR1 dependency in squamous cell lung cancer. *Sri Transl Med*. 2010; 2:62ra93.
6. Bass AJ, Watanabe H, Mermel CH, Yu S, Perner S, Verhaak RG, et al. SOX2 is an amplified lineage-survival oncogene in lung and esophageal squamous cell carcinomas. *Nat Genet*. 2009; 41:1238–42. [PubMed: 19801978]
7. Hammerman PS, Sos ML, Ramos AH, Xu C, Dutt A, Zhou W, et al. Mutations in the DDR2 kinase gene identify a novel therapeutic target in squamous cell lung cancer. *Cancer Discov*. 2011; 1:78–89. [PubMed: 22328973]
8. Castillo SD, Angulo B, Suarez-Gauthier A, Melchor L, Medina PP, Sanchez-Verde L, et al. Gene amplification of the transcription factor DP1 and CTNND1 in human lung cancer. *J Pathol*. 2010; 222:89–98. [PubMed: 20556744]
9. Cancer T, Atlas G. Comprehensive genomic characterization of squamous cell lung cancers. *Nature*. 2012; 489:519–25. [PubMed: 22960745]
10. Hamada K, Kohno T, Kawanishi M, Ohwada S, Yokota J. Association of CDKN2A (p16)/CDKN2B (p15) alterations and homozygous chromosome arm 9p deletions in human lung carcinoma. *Genes Chromosom Cancer*. 1998; 22:232–40. [PubMed: 9624535]
11. Sanchez-Cespedes M. A role for LKB1 gene in human cancer beyond the Peutz-Jeghers syndrome. *Oncogene*. 2007; 26:7825–32. [PubMed: 17599048]
12. Rothenberg SM, Mohapatra G, Rivera MN, Winokur D, Greninger P, Nitta M, et al. A genome-wide screen for microdeletions reveals disruption of polarity complex genes in diverse human cancers. *Cancer Res*. 2010; 70:2158–64. [PubMed: 20215515]

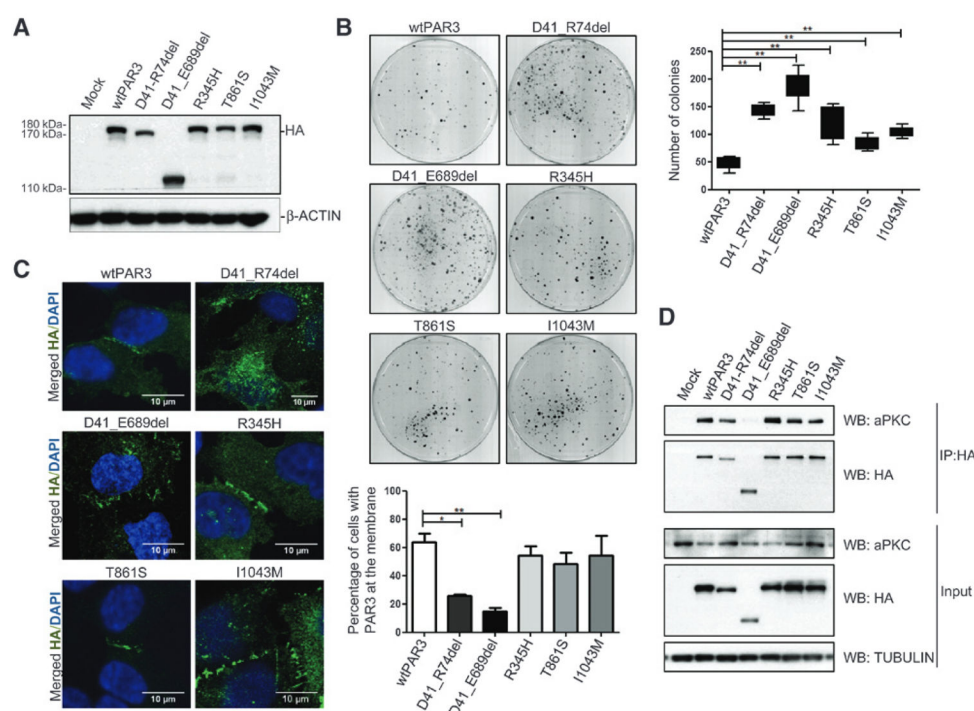
13. Kemphues KJ, Priess JR, Morton DG, Cheng NS. Identification of genes required for cytoplasmic localization in early *C. elegans* embryos. *Cell*. 1988; 52:311–20. [PubMed: 3345562]
14. Goldstein B, Macara IG. The PAR proteins: fundamental players in animal cell polarization. *Dev Cell*. 2007; 13:609–22. [PubMed: 17981131]
15. Laprise P, Tepass U. Novel insights into epithelial polarity proteins in *Drosophila*. *Trends Cell Biol*. 2011; 7:401–8. [PubMed: 21530265]
16. Martin-Belmonte F, Perez-Moreno M. Epithelial cell polarity, stem cells and cancer. *Nat Rev Cancer*. 2012; 12:23–38. [PubMed: 22169974]
17. Iden S, van Riel WE, Schäfer R, Song J-Y, Hirose T, Ohno S, et al. Tumor type-dependent function of the par3 polarity protein in skin tumorigenesis. *Cancer Cell*. 2012; 22:389–403. [PubMed: 22975380]
18. McCaffrey LM, Montalbano J, Mihai C, Macara IG. Loss of the Par3 polarity protein promotes breast tumorigenesis and metastasis. *Cancer Cell*. 2012; 22:601–14. [PubMed: 23153534]
19. Leong PP, Rezai B, Koch WM, Reed A, Eisele D, Lee D, et al. Distinguishing second primary tumors from lung metastases in patients with head and neck squamous cell carcinoma. *J Natl Cancer Inst*. 1998; 90:972–7. [PubMed: 9665144]
20. Xi T, Jones IM, Mohrenweiser HW. Many amino acid substitution variants identified in DNA repair genes during human population screenings are predicted to impact protein function. *Genomics*. 2004; 83:970–9. [PubMed: 15177551]
21. Knudson AG. Mutation and cancer: statistical study of retinoblastoma. *Proc Natl Acad Sci U S A*. 1971; 68:820–3. [PubMed: 5279523]
22. Aranda V, Nolan ME, Muthuswamy SK. Par complex in cancer: a regulator of normal cell polarity joins the dark side. *Oncogene*. 2008; 27:6878–87. [PubMed: 19029931]
23. Georgiou M, Baum B. Polarity proteins and Rho GTPases cooperate to spatially organise epithelial actin-based protrusions. *J Cell Sci*. 2010; 123:1089–98. [PubMed: 20197404]
24. Pegtel DM, Ellenbroek SIJ, Mertens AEE, van der Kammen RA, de Rooij J, Collard JG. The Par-Tiam1 complex controls persistent migration by stabilizing microtubule-dependent front-rear polarity. *Curr Biol*. 2007; 17:1623–34. [PubMed: 17825562]
25. Chen X, Macara IG. Par-3 controls tight junction assembly through the Rac exchange factor Tiam1. *Nat Cell Biol*. 2005; 7:262–9. [PubMed: 15723052]
26. Rock KL, Gramm C, Rothstein L, Clark K, Stein R, Dick L, et al. Inhibitors of the proteasome block the degradation of most cell proteins and the generation of peptides presented on MHC class I molecules. *Cell*. 1994; 78:761–71. [PubMed: 8087844]
27. Dabir S, Kluge A, McColl K. PIAS3 activates the intrinsic apoptotic pathway in non-small cell lung cancer cells independent of p53 status. *Int J Cancer*. 2014; 134:1045–54. [PubMed: 23959540]
28. Raptis L, Arulanandam R, Geletu M, Turkson J. The R(h)oads to Stat3: Stat3 activation by the Rho GTPases. *Exp Cell Res*. 2011; 317:1787–95. [PubMed: 21619876]
29. Steinman RA, Wentzel A, Lu Y, Stehle C, Grandis JR. Activation of Stat3 by cell confluence reveals negative regulation of Stat3 by cdk2. *Oncogene*. 2003; 22:3608–15. [PubMed: 12789269]
30. Vultur A, Cao J, Arulanandam R, Turkson J, Jove R, Greer P, et al. Cell-to-cell adhesion modulates Stat3 activity in normal and breast carcinoma cells. *Oncogene*. 2004; 23:2600–16. [PubMed: 15007380]
31. Vareille M, Kieninger E, Edwards MR, Regamey N. The airway epithelium: soldier in the Fight against respiratory viruses. *Clin Microbiol Rev*. 2011; 24:210–29. [PubMed: 21233513]
32. Schumann M, Günzel D, Buerger N, Richter JF, Troeger H, May C, et al. Cell polarity-determining proteins Par-3 and PP-1 are involved in epithelial tight junction defects in coeliac disease. *Gut*. 2012; 61:220–8. [PubMed: 21865402]
33. Mizuno K, Suzuki A, Hirose T, Kitamura K, Kutsuzawa K, Futaki M, et al. Self-association of PAR-3-mediated by the conserved N-terminal domain contributes to the development of epithelial tight junctions. *J Biol Chem*. 2003; 278:31240–50. [PubMed: 12756256]
34. Sanchez-Cespedes M, Parrella P, Esteller M, Nomoto S, Trink B, Engles JM, et al. Inactivation of LKB1/STK11 is a common event in adenocarcinomas of the lung. *Cancer Res*. 2002; 62:3659–62. [PubMed: 12097271]

35. Vahtomeri K, Mäkelä TP. Molecular mechanisms of tumor suppression by LKB1. *FEBS Lett.* 2011; 585:944–51. [PubMed: 21192934]
36. Benton R, Johnston DS. A conserved oligomerization domain in drosophila Bazooka/Par-3 is important for apical localization and epithelial polarity. *Curr Biol.* 2003; 13:1330–4. [PubMed: 12906794]
37. Lin D, Edwards AS, Fawcett JP, Mbamalu G, Scott JD, Pawson T. A mammalian PAR-3-PAR-6 complex implicated in Cdc42/Rac1 and aPKC signalling and cell polarity. *Nat Cell Biol.* 2000; 2:540–7. [PubMed: 10934475]
38. Nakayama M, Goto TM, Sugimoto M, Nishimura T, Shinagawa T, Ohno S, et al. Rho-kinase phosphorylates PAR-3 and disrupts PAR complex formation. *Dev Cell.* 2008; 14:205–15. [PubMed: 18267089]
39. Ishiuchi T, Takeichi M. Willin and Par3 cooperatively regulate epithelial apical constriction through aPKC-mediated ROCK phosphorylation. *Nat Cell Biol.* 2011; 13:860–6. [PubMed: 21685893]
40. Hidalgo-Carcedo C, Hooper S, Chaudhry SI, Williamson P, Harrington K, Leitingner B, et al. Collective cell migration requires suppression of actomyosin at cell-cell contacts mediated by DDR1 and the cell polarity regulators Par3 and Par6. *Nat Cell Biol.* 2011; 13:49–58. [PubMed: 21170030]
41. Wang C, Su H, Hsu Y, Shen M, Tang M. A discoidin domain receptor 1/SHP-2 signaling complex inhibits alpha2beta1-integrin-mediated signal transducers and activators of transcription 1/3 activation and cell migration. *Mol Biol Cell.* 2006; 17:2839–52. [PubMed: 16611743]
42. Simon AR, Vikis HG, Stewart S, Fanburg BL, Cochran BH, Guan KL. Regulation of STAT3 by direct binding to the Rac1 GTPase. *Science.* 2000; 290:144–7. [PubMed: 11021801]
43. Koskela HLM, Eldfors S, Ellonen P, van Adrichem AJ, Kuusanmäki H, Andersson EI, et al. Somatic STAT3 mutations in large granular lymphocytic leukemia. *N Engl J Med.* 2012; 366:1905–13. [PubMed: 22591296]
44. Couto JP, Daly L, Almeida A, Knauf JA, Fagin JA, Sobrinho-Simões M, et al. STAT3 negatively regulates thyroid tumorigenesis. *Proc Natl Acad Sci U S A.* 2012; 109:E2361–70. [PubMed: 22891351]
45. Kuo TH, Kubota T, Watanabe M, Furukawa T, Kase S, Tanino H, et al. Site-specific chemosensitivity of human small-cell lung carcinoma growing orthotopically compared to subcutaneously in SCID mice: the importance of orthotopic models to obtain relevant drug evaluation data. *Anticancer Res.* 1993; 13:627–30. [PubMed: 8391244]
46. Ambrogio C, Carmona FJ, Vidal A, Falcone M, Nieto P, Romero OA, et al. Modeling lung cancer evolution and therapeutic response by orthotopic mouse allografts. *Cancer Res.* 2014; 74:5978–88. [PubMed: 25217522]

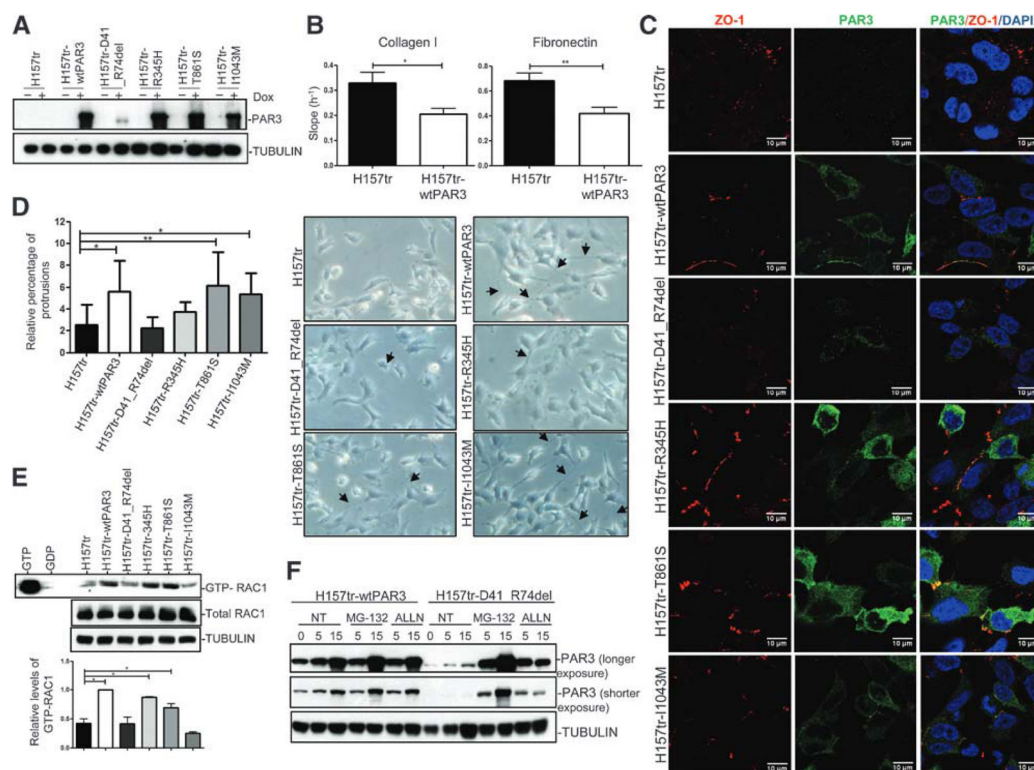
**Figure 1.**

PARD3-inactivating mutations in LSCCs. A, mutations of the PC10 cells at the genomic DNA (gDNA) and mRNA (cDNA) level. B, mutation in a lung tumor but not in the matched normal DNA. D10S1780 designates one microsatellite marker showing LOH. The agarose gel depicts the deletion of exon 2 in this tumor at the mRNA level. C, top, representation of the structure of PARD3, highlighting the location of the exons deleted (red). Bottom, ratio charts of the MLPA depicting the deletion of exons 2 to 13 (top) and of the normal matched DNA (bottom). Right plots, shorter transcript arising from the deletion. The D10S1780 depicts the presence of LOH. D, representation of the PAR3 protein structure and the location of those PARD3 mutations that do not predict truncated proteins. aPKCb, atypical protein kinase C binding site; CC, coiled coil domains; CR1, control region 1; PDZ, PDZ domains.



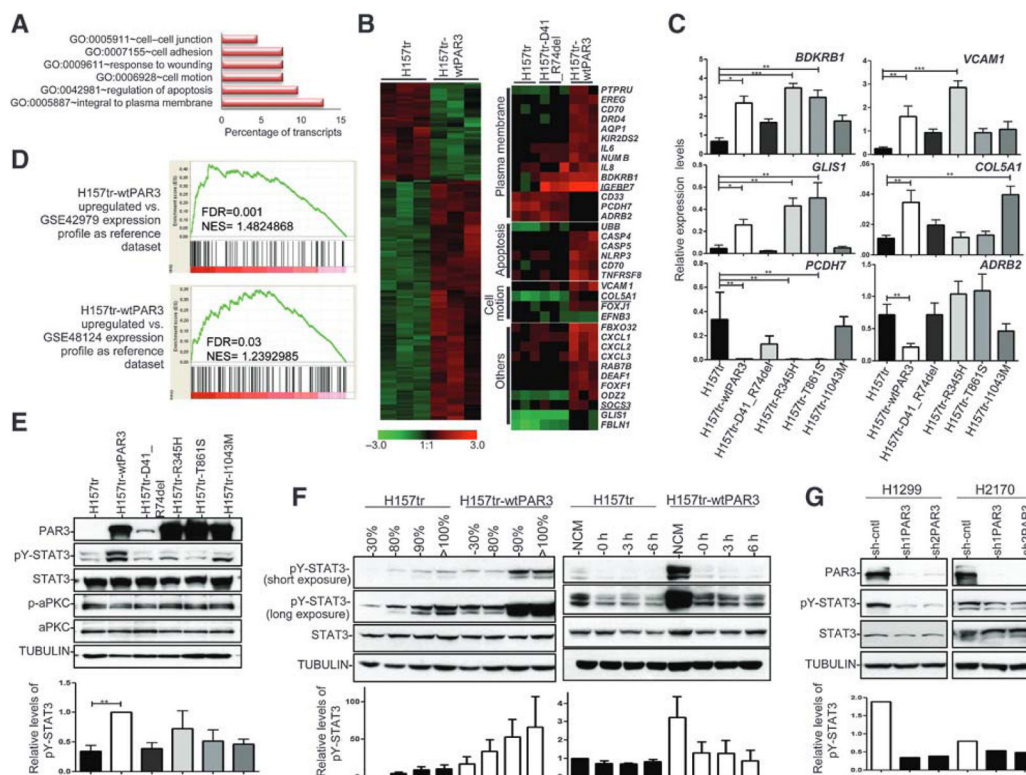
**Figure 2.**

Effects of the PAR3-mutant proteins on cell growth inhibition, protein localization, and binding to aPKC. A, Western blot shows ectopic expression of the various PAR3 proteins. β-ACTIN, protein-loading control. B, restitution of wtPAR3 significantly reduces colony formation in H157 cells. Right, quantification of the assay. C, immunofluorescence to determine localization of PAR3. Right, quantification of the assay. Error bars, SD. D, coimmunoprecipitation of aPKC with anti-HA from extracts of the H157 cells expressing the indicated proteins. One twentieth of the input lysate and of the immunoprecipitated (IP) fraction were immunoblotted (WB) with hemagglutinin or aPKC antibodies. TUBULIN, protein-loading control. \*,  $P < 0.05$ ; \*\*,  $P < 0.01$ .

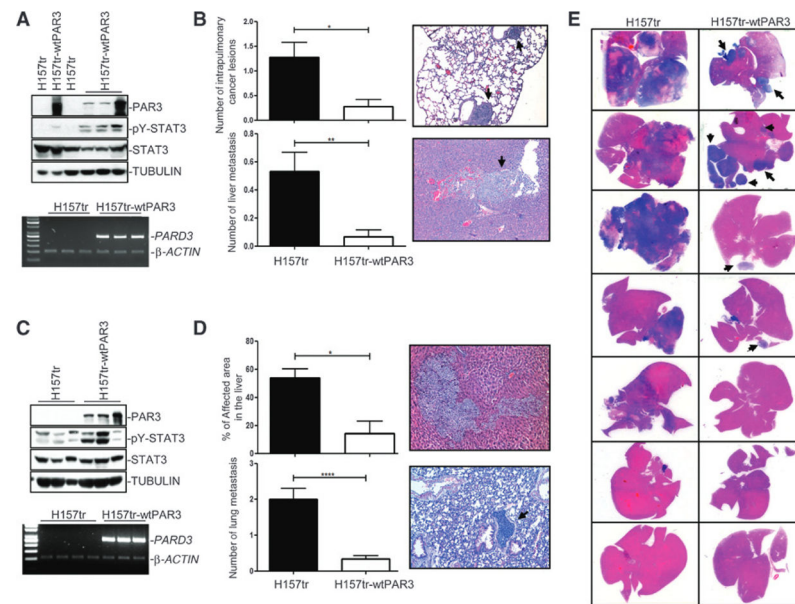
**Figure 3.**

Effects of the wtPAR3 and PAR3-mutant proteins on various polarity related parameters. A, Western blot of PAR3, stably expressed under a tet-repressor-controlled vector. Presence (+) or absence (–) of doxycycline (dox, 1 ng/μL; 24 h). TUBULIN, protein-loading control. B, xCELLigence system assay, using collagen I or fibronectin. Error bars, SD. \*,  $P < 0.05$ ; \*\*,  $P < 0.01$ . C, immunofluorescence of PAR3 and ZO-1. Nuclei were stained with DAPI. D, right, phase-contrast images of the indicated cells 24 hours after seeding. Arrows, protrusions. Left, quantification of the percentage of protrusions relative to the total number of cells.

E, amounts of GTP-RAC1 and total RAC1 determined by immunoblotting with anti-RAC1 antibody. Positive (GTP) and negative (GDP) controls are included. Bottom, relative ratio of RAC1-GTP to total RAC1, normalized with respect to the wt value. F, Western blots of PAR3, following treatment with either MG132 or ALLN, for the indicated times (hours) after induction with doxycycline. NT, untreated cells.

**Figure 4.**

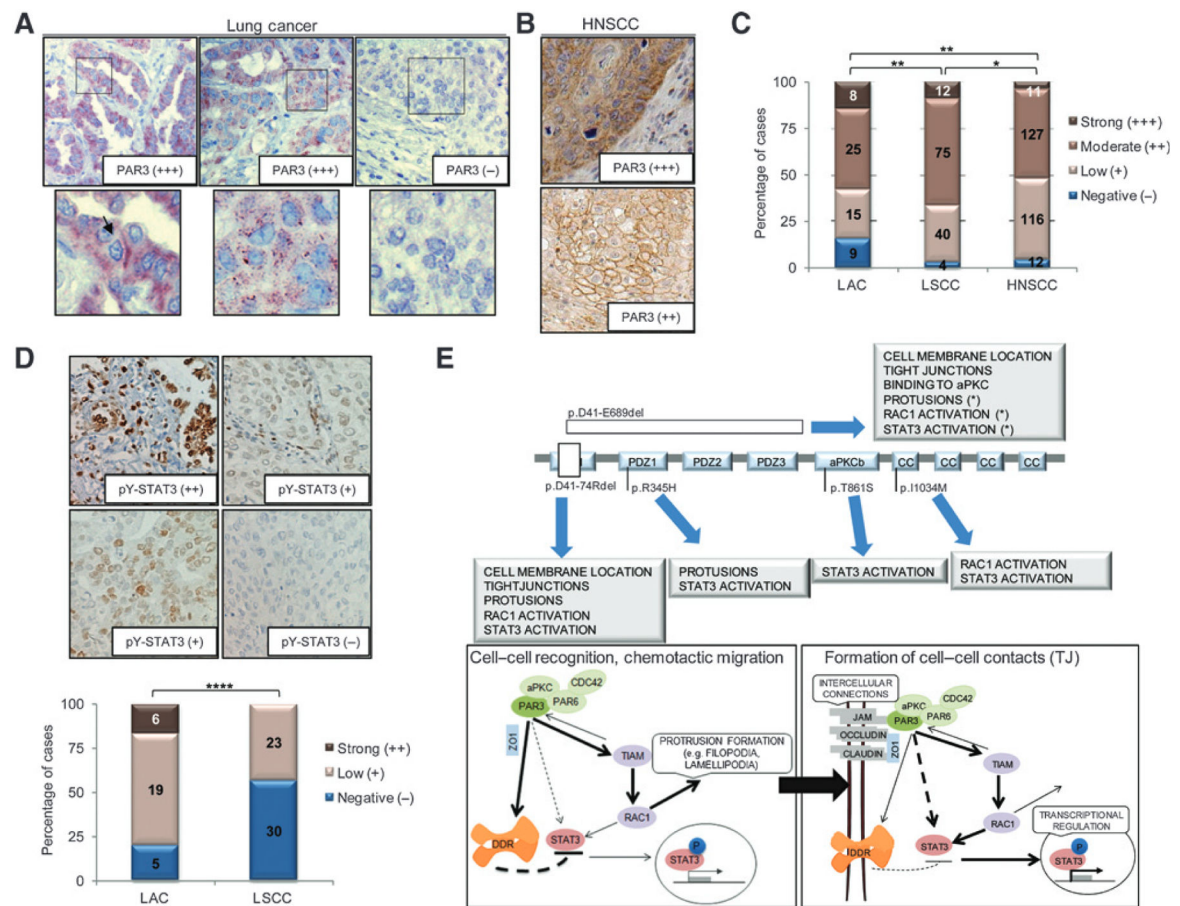
Gene expression signature of PAR3. A, enriched gene ontology (GO) classifications ( $P < 0.05$ ) among genes upregulated by PAR3 (Supplementary Table S5). B, left, heatmap of the transcripts comprising the PAR3 gene expression signature. Right, heatmap of selected genes from each indicated gene ontology category. C, mRNA levels assessed by real-time quantitative PCR of representative transcripts (relative to ACTB). Error bars, SD. \*,  $P < 0.05$ ; \*\*,  $P < 0.01$ ; \*\*\*,  $P < 0.005$ . D, graph of the ranked gene lists from the Gene Set Enrichment Analysis (GSEA) comparisons. Probabilities and FDRs are indicated. E, top, Western blot depicting levels of the indicated proteins after induction of PAR3 expression (doxycycline, 1 ng/ $\mu$ L; 24 h). F, Western blot of the indicated proteins. Left, cells grown to different degrees of confluence. Right, calcium switch assay; 0, 3, and 6 hours after readdition of calcium; NCM, normal calcium-containing medium. G, Western blot depicting the downregulation of PAR3 levels, with two independent shRNAs (sh#1/sh#2). sh-cntl, scramble control. TUBULIN, protein-loading control. E–G, bottom panels, densitometric analysis to quantify the levels of pY-STAT3 relative to total STAT3.



**Figure 5.**

PAR3 expression decreased tumor cell invasiveness and metastasis, in vivo. A, the H157tr and the H157tr-wtPAR3 cells were grown orthotopically in athymic nude mice (45, 46). Representative Western blots (top) and RT-PCRs (bottom) of the induction of PAR3 in lung orthotopic tumors. The levels of pY-STAT3 are also shown. TUBULIN, protein-loading control. B, mean frequency of intrapulmonary cancer lesions and liver metastases in each group. Error bars, SDs. Right, representative hematoxylin and eosin preparations of the metastases (arrow) in the lung and liver (magnification,  $\times 100$ ). C, cells were implanted in the spleen. Representative Western blot (top) and RT-PCR (bottom) of the induction of PAR3 in tumors derived from the indicated cancer cells. Levels of pY-STAT3 and of total STAT3 are also shown. D, left, mean frequency of intrapulmonary metastases and the area of the liver affected by metastasis. Error bars, SD. Right, representative hematoxylin and eosin preparations of the metastases (arrows; magnification,  $\times 100$ ). E, hematoxylin and eosin staining of liver metastasis in the splenic mouse model. Purple and pink areas, tumor and normal liver cells, respectively. In the left column, the third and fourth images from top to bottom correspond to a single tumor from the same animal. Arrows, well-defined and round-shaped cancer lesions. B and D, \*,  $P < 0.05$ ; \*\*,  $P < 0.01$ ; \*\*\*\*,  $P < 0.001$ .



**Figure 6.**

PAR3 immunostaining in lung and HNSCC primary tumors. A, top, representative immunostainings of PAR3 in lung tumors (magnification,  $\times 200$ ). Bottom plots are insets from the indicated pictures. Arrows, cells showing PAR3 localization at the cell edge. B, immunostaining of PAR3 in HNSCC (magnification,  $\times 200$ ). C, bar graphs, distribution of LACs, LSCCs, and HNSCCs by PAR3 immunostaining categories. Inside the bars, number of tumors within each category. D, top, representative immunostainings of pY-STAT3 in lung tumors (magnification,  $\times 200$ ). Bottom, bar graphs showing the distribution of lung AC and SCC by pY-STAT3 immunostaining categories. E, top, representation of PAR3, showing the mutations and the functionalities of PAR3 that are affected in each case. (\*), effects on the functionalities of PAR3 are inferred from the observations made for the p.D41\_R74del protein. Bottom, representation of cell processes that require PAR3 and of the downstream targets activated in each case. Left, wtPAR3 promotes the formation of protrusions, allowing the sensation of chemotrophic cues that will result in substrate adhesion and in directed locomotion toward establishing contacts between cells. This would involve the activation of RAC1 but not of STAT3. Right, the proximity of neighboring cells promotes the formation of a tight junction (TJ) by a PAR3-dependent process. This triggers the activation of both RAC1 and STAT3. Thus, the absence of wtPAR3 subverts the mechanisms of recognition and interaction between neighboring cells. This can be deleterious for most epithelial tissues, including the respiratory epithelia, which rely strongly

on tight junctions for maintaining their integrity. C and D, \*,  $P < 0.05$ ; \*\*,  $P < 0.01$ ; \*\*\*,  $P < 0.001$ .

Author Manuscript

Author Manuscript

Author Manuscript

Author Manuscript



Table 1

PARD3 gene alterations found in lung cancer cell lines and in lung primary squamous cell carcinomas

Identification	Nucleotide change	Predicted effect	Exon/intron	Status	Somatic	Predicted impact <sup>a</sup>
LSCC cancer cell lines (n = 18)						
NCI-H157	c.715-?_2614+?del	No protein	E6-E18	LOH	NA	NA
PC10	c.223-4C>G	No protein	I2	NO LOH	NA	NA
PC10	c.2581A>T	p.T861S	E18	NO LOH	NA	Damaging
LSCC primaries (N = 108)						
1681 (T1)	c.223-?_3549+?del	No protein	E3-23	LOH	Yes	NA
141 (T2) <sup>b</sup>	c.121-2A>G	p.D41_R74del	II	LOH	Yes	NA
181 (T3) <sup>b</sup>	c.404-?_582+?del	No protein	E4	NA	NA	NA
269 (T4)	c.1034G>A	p.R345H	E9	LOH	Yes	Damaging
200 (T6)	c.1492insG	p.A498Gfs*9	E10	LOH	Yes	NA
273 (T7)	c.3129A>G	p.I1043M	E21	LOH	Yes	Benign
114 (T8) <sup>b</sup>	c.121-?_2067+?del	p.D41_E689del	E2-E13	LOH	Yes	NA
1529 (T9)	c.404-?_3549+?del	No protein	E4-E23	LOH	Yes	NA

NOTE: Ref Seq, mRNA sequence NM. 019619.

Abbreviation: NA, not analyzable.

<sup>a</sup> PolyPhen impact.

<sup>b</sup> Confirmed at mRNA level.